

Kinetic Modelling of Impurity Transport in Detached Plasma for Integrated Divertor Simulation with SONIC (SOLDOR/NEUT2D/IMPMP/EDDY)

K. Shimizu 1), T. Takizuka 1), K. Ohya 2), K. Inai 2), T. Nakano 1), A. Takayama 3),
H. Kawashima 1), K. Hoshino 1)

1) Japan Atomic Energy Agency, Naka, Ibaraki-ken, 311-0193 Japan

2) The University of Tokushima, Tokushima 770-8506, Japan

3) National Institute for Fusion Science, Toki 509-5292, Japan

e-mail contact of main author: shimizu.katsuhiko@jaea.go.jp

Abstract. An integrated divertor simulation code SONIC has been developed. The self-consistent coupling of an MC impurity code IMPMP to a divertor code SOLDOR/NEUT2D is succeeded by overcoming the intrinsic problems of Monte Carlo (MC) modelling for impurity transport. MC modelling for impurity transport is required in order to take into account the kinetic effect and the complex dissociation processes of hydrocarbons. The integrated divertor code SONIC enables us to investigate the details of impurity transport including erosion/redeposition processes on the divertor plates by further coupling of an MC code EDDY. The dynamic evolution of X-point MARFE observed in JT-60U is investigated. The simulation results indicate that the hydrocarbons sputtered from the dome contribute directly to the enhanced radiation near the X-point. Without the recycling, the kinetic effect of the thermal force improves the helium compression, compared with the conventional (fluid) evaluation. This effect is, however, masked by the recycling at the divertor targets.

1. Introduction

Control of the power and particle is one of the most critical issues to achieve the fusion reactors, such as ITER. To investigate the control method by the divertor, 2D multi-fluid divertor codes have been developed, where the impurities are treated usually as fluid species [1]. The fluid modelling for the impurity transport contains the improper descriptions; (1) assumption of instantaneous thermalization of impurity ions, (2) neglecting the kinetic effect on the thermal force and (3) simplification for the complicated dissociation process of hydrocarbons. The MC approach is suitable for such effects to be taken into account [2]. However, it has the disadvantage of (i) long computational time, (ii) large MC noise, and (iii) assumption of steady state. Thus, time-evolutional simulation with an MC impurity code coupled self-consistently to a plasma fluid code has not been presented so far. We solved the first and the second problems of MC modelling by developing a new diffusion model for scattering process and optimizing on the massive parallel computer [3]. Recently, we solved the last problem by extending the IMPMP to a time-dependent simulation code, where increasing number of test particles with time is suppressed by a particle reduction scheme [4]. Thereby we have accomplished a coupling of non-steady IMPMP [5] code into a 2D divertor code (SOLDOR/NEUT2D) [6]. We carry out the simulations with the SONIC code for penetration process of hydrocarbons into the main plasma and helium compression in the detached plasma and find out the importance of the kinetic effect in the impurity transport.

2. Model Development

We are developing a self-consistent modelling of divertor plasma and impurity transport. The integrated divertor code package consists of the 2D fluid code for plasma (SOLDOR) [6], the neutral Monte-Carlo code (NEUT2D) and the impurity Monte-Carlo code (IMPMP) [5]. The key feature of this integrated code, SONIC, is to incorporate the elaborate impurity Monte

Carlo code, IMPMC. Monte-Carlo (MC) approach is suitable for modelling of interactions between impurities and walls, including kinetic effects, and the complicated dissociation process of hydrocarbons. However, there needs to overcome the intrinsic problems of MC modelling so that it is consistently coupled with the divertor code. The model developments to solve these problems and the kinetic modelling are described in this section.

2.1 Diffusion Model for Scattering Process in Detached Plasma

When a conventional MC algorithm is employed for scattering process in velocity space, the impurity ions must be traced with a time step Δt much shorter than the slowing-down time τ_s . In consequence, the MC code requires a huge amount of computational time, especially in case of detached plasma because of extremely short slowing-down time, typically, $\tau_s \sim 10^{-8}$ s for C^{3+} in the detached plasma of $n_e \sim 1 \times 10^{20} \text{ m}^{-3}$, $T_e = T_i \sim 1$ eV. The impurity ions diffuse in the velocity space (VD model) by Coulomb collisions, and the spatial diffusion parallel to the magnetic field line arises from the change of parallel velocity due to collisions. These processes are described by the Langevin equations. We developed a new diffusion model using analytical solution of Langevin equations [3]. In the new diffusion model, the position (s) and the parallel velocity (v) of a test particle can be chosen from the normal distributions with two normal random numbers, r_{G1} and r_{G2} .

$$\begin{aligned} s(t) &= \mu_s(t) + \sigma_s(t) \cdot r_{G1} \\ v(t) &= \mu_v(t) + \sigma_v(t) \cdot r_{G2} \end{aligned} \quad (1)$$

Here μ is the mean, σ is the standard deviation, which are given as analytical solution. The computational time is significantly reduced by this new algorithm, typically more than 100 times faster than the conventional MC method.

2.2 Particle Reduction Scheme

In time-dependent simulation with MC code, a serious problem arises: number of test particles increases with time. It strongly depends on the impurity retention and the duration of simulation. When the number of test particles attains to $10^6 \sim 10^7$, simulations require unexpectedly long computational time. Therefore, it is necessary for the efficient simulation to suppress the number of test particles in MC calculation. In a typical simulation of carbon impurity due to physical sputtering, half of test particles exist in the core plasma ($r/a < 0.95$) and the density of impurity ions is uniform there in poloidal direction. Excessive test particles in the main plasma are unnecessary. Particle reduction, therefore, is performed for C^{6+} particles in the core region. A ‘‘particle reduction scheme’’ was established [4]. Its process consists of three steps; sorting of weight, pairing, and Russian roulette. Russian roulette decides which particle of the pair to be terminated. Reducing total particle number from 1.1×10^6 to 0.36×10^6 , it leads to increase the variance in the local impurity density. However, the MC noise remains in a permissible level.

2.3 Dissociation Process of Hydrocarbons

The erosion of the wall related to lifetime of divertor component and tritium retention in the device are crucial issues for ITER. In order to study minutely such processes, the EDDY code has been developed [7]. The code is a 3D Monte Carlo impurity code, which contains the following processes; (1) physical and chemical sputtering, which are released methane and higher hydrocarbons, (2) ionization and complex dissociation processes using the data

produced by Janev and Reiter [8], (3) 3 dimensional motion of ions acted on by the magnetic field, the electric field including the sheath and presheath acceleration, the friction force and thermal force, (4) anomalous cross field diffusion, (5) elastic collision with neutral hydrogen and (6) energy- and species-dependent reflection model. In addition, the EDDY code can simulate dynamic material mixing processes, which is distinct from other codes. The gyro motion of ion is followed to evaluate the prompt redeposition, in contrast with the IMPMC code where the guiding-center approximation is employed. Since the purpose of the EDDY code is to investigate the erosion and redeposition processes, the tracking of test particles is confined to the vicinity of the divertor targets. In order to investigate the contamination process into the main plasma and migration of carbon impurity in large scale, we have developed a coupling code of EDDY and IMPMC. To save computational time, when the test particles are ~ 1 cm (\gg Larmor radius) away from the target plates, their guiding-center motion are traced with the IMPMC code. Conversely, when the test particles move into the vicinity of the targets, they are traced with the EDDY code, taking into account the interaction with the targets.

2.4 Kinetic Thermal Force

The impurity retention in the divertor region is basically determined by the balance between the thermal force (toward hotter region in fluid approximation) and the friction force (toward divertor plates). Using a drift kinetic model, the kinetic thermal force was derived by Reiser et al. [9]. In contrast with the fluid thermal force which is averaged over a Maxwellian velocity distribution of impurity ions, the kinetic thermal force was found to have the opposite direction (towards colder region) for impurity ions with high speeds. We independently derived an expression of the kinetic thermal force [10]. The ion thermal force is defined by

$$\bar{\mathbf{R}}_{\nabla T_i} = \int m_i \mathbf{v} C(f_i, \delta f_i) d\mathbf{v} \quad (2)$$

where C is the Fokker-Planck collision operator, f_i is the distribution function of impurity ions, δf_i is the ion distribution function distorted by the ion temperature gradient ∇T_i . Substituting $f_i(\mathbf{v}) = \delta(\mathbf{v} - \mathbf{V}_0)$ into Eq. (2), we obtain the force along the magnetic field line acting on an impurity ion with a velocity of \mathbf{V}_0

$$F_{\nabla T_i}(\mathbf{V}_0) \equiv \int d\mathbf{v}' \delta f_i(\mathbf{v}') m_i \{ \Delta \mathbf{v}_{//} \}_i = \int d\mathbf{v}' \delta f_i(\mathbf{v}') \left\{ -\frac{4\pi\lambda e^4 Z_i^2 Z_I^2}{m_{ii}} \frac{\mathbf{u} \cdot \mathbf{b}}{u^3} \right\} \quad (3)$$

where m_{ii} is the reduced mass, $\mathbf{u} = \mathbf{V}_0 - \mathbf{v}'$, \mathbf{b} the unit vector along the magnetic field line. Braginskii derived the distorted distribution function by use of Laguerre polynomials [11].

$$\delta f_i(\mathbf{v}) = \frac{n_i}{\pi^{3/2} v_{th}^3} \exp\left(-\frac{m_i}{2T_i} v^2\right) \cdot \tau_i \sum_{n=1}^N a_n L_n^{(3/2)}\left(\frac{m_i}{2T_i} v^2\right) \cdot (\mathbf{v} \cdot \nabla_{//} \ln T_i) \quad (4)$$

where coefficients a_n are $a_1 = \frac{26895}{17056}$, $a_2 = \frac{1525}{3198}$, $a_3 = \frac{35}{533}$. The integration of Eq. (3) is carried out numerically by using the Gauss-Legendre integral method. Figure 1 shows the kinetic thermal force acting on a particle with $\alpha=30$ degree, where α is an angle between velocity and

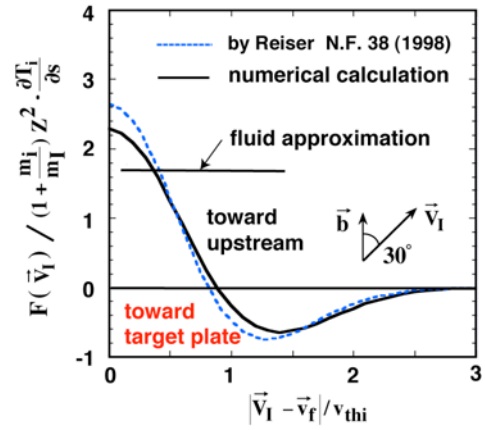


FIG. 1 Kinetic thermal force. It changes direction according to impurity speed.

the magnetic field line. The kinetic thermal force derived analytically by Reiser et al. is shown by a broken line. Our result agrees well with their theoretical one. The kinetic effect may influence impurity density profile a little, because the impurity speed is usually much lower than the background thermal speed. The condition possibly changes for the He ion transport in detached divertor region, where He^{2+} ions inflow across the separatrix surface into the SOL region with high speeds and subsequently flow into the cold divertor region. In this situation, the normalized He ion speed may become $V_0/v_{\text{thi}} \geq 1$.

3. Simulation of Impurity Behavior at X-point MARFE

The contamination process of carbon impurity into the main plasma is investigated in JT-60U detached divertor plasmas. Simulations are carried out for the high-density discharge with a strong D_2 gas puffing and neutral-beam heating ($R=3.3\text{m}$, $a=0.9\text{m}$, $\kappa=0.95$, $I_p=1.5\text{MA}$, $B_T=3\text{T}$, $P_{\text{NB}}=15\text{MW}$). The strong gas puffing induced an X-point MARFE. As simulation parameters in the SOLDOR/NEUT2D, the heat flux and the particle flux from the core edge ($r/a=0.95$) are assumed to be $Q_i=Q_e=7\text{MW}$, $\Gamma_i=3 \times 10^{21} \text{ s}^{-1}$. We employ $D_{\perp}=0.25 \text{ m}^2/\text{s}$ for the anomalous particle diffusion coefficient and $\chi_{\perp}^i=\chi_{\perp}^e=1 \text{ m}^2/\text{s}$ for the anomalous thermal diffusivities. The recycling coefficient at the divertor plates and walls is set to 1.0 for both ion and neutral particles. The albedo for neutral particles at the pumping port is specified so that the pumping speed is $S_{\text{pump}}=26 \text{ m}^3/\text{s}$. In the IMPMC calculation, the carbon outfluxes due to physical and chemical sputtering are determined self-consistently taking account of sputtering yields and incident fluxes of deuterium ions and neutrals onto the target plates and the walls. Here the EDDY code is not yet coupled. An attached divertor plasma is obtained in a steady state before the gas puff, where the radiation of carbon concentrates near both strike points (Fig. 2(a)). After a strong gas puff of $\Gamma_{\text{puff}}=6 \times 10^{22} \text{ s}^{-1}$, the radiation profile changes temporally as shown in Fig. 2(b)–(c). The radiation peaks move away from the strike point and shift upstream slightly in a partially detached plasma (Fig. 2(b)). The region with high radiation power extends from the strike point up to near the X-point along the separatrix. In the X-point MARFE phase, the radiation peaks shift to near the X point as shown in Fig. 2(c). The density at the X-point attains to $7 \times 10^{20} \text{ m}^{-3}$ and the electron temperature becomes low ($\sim 2 \text{ eV}$). This evolution of radiation profile agrees fairly well with that observed in JT-60U experiments with a strong gas puffing [12]. In the detached plasma, a part of carbon sputtered from the dome penetrates directly into the main plasma because the electron temperature in the private region is becomes around 1~2 eV. These carbons contribute to the enhanced radiation near the X-point.

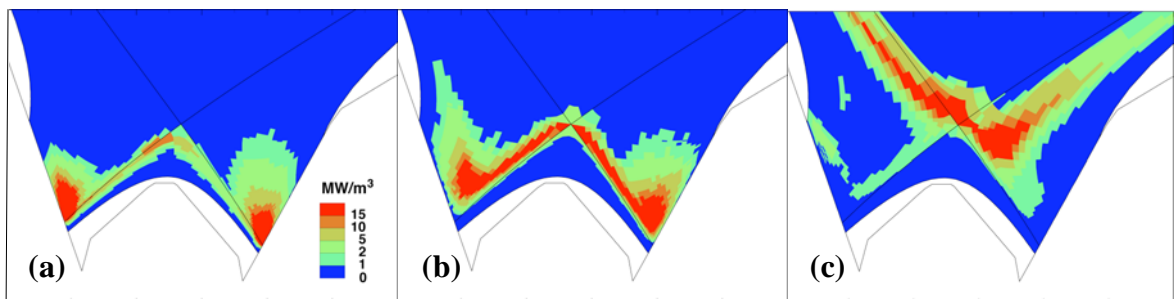


FIG. 2 Radiation profiles calculated with SOLDOR/NEUT2D/IMPMC for (a) attached plasma before strong gas puffing, (b) detached plasma after strong gas puffing, and (c) X-point MARFE. Simulation results reproduce the dynamic evolution of X-point MARFE observed in JT-60U high density discharge.

4. EDDY/IMPIC Simulation

In the above simulations, the complex dissociation processes of CD_4 are simplified down to an ionization process of C with a low energy ($\sim 1\text{eV}$), as widely used in other divertor code. This approximation is examined by using the EDDY/IMPIC code, where the methane breakup processes and the reflection at the divertor target are taken into account. Simulations are carried out for a typical plasma with the detached inner divertor ($n_{ed} = 4.2 \times 10^{20} \text{ m}^{-3}$, $T_{ed} = 1.7 \text{ eV}$ at the strike point) and the attached outer divertor ($n_{ed} = 1.9 \times 10^{20} \text{ m}^{-3}$, $T_{ed} = 17 \text{ eV}$ at the strike point). The erosion and redeposition patterns on the JT-60U divertor were calculated with the EDDY code. From comparison with the experimental results, it was found that the sticking coefficient of hydrocarbons on the outer divertor target was small [7]. To investigate the effect of dissociation process on the carbon transport without complicated argument, the sticking coefficient is assumed to be zero on both the inner and outer targets. From either the inner or outer strike point, 5000 test particles are emitted and are traced until they are dissociated/ionized to C^+ ions. Fig. 3(a) shows the birth position of C^+ ions from dissociation of CD_4 and Fig. 3(b) shows the birth position from ionization of C emitted with an energy of $\sim 1 \text{ eV}$. Because of low electron temperature in the detached divertor, half of the emitted CD_4 can path through the private region, strike on the dome and are reflected as neutral hydrocarbons. The neutral hydrocarbons are further dissociated near the separatrix and strike on the dome again. These processes are repeated. As a result, carbon ions are spread out along the separatrix. The behavior of neutral carbons is similar as shown in Fig.3 (b). However, the dissociation processes of CD_4 emitted from the outer strike point differs considerably from the ionization process of C. Almost all ionizations of C neutral is located adjacent the outer strike point due to high ionization cross section ($T_e \sim 20 \text{ eV}$). On the other hand, the fragments of hydrocarbon get the dissociation energy and some neutral hydrocarbon with a high-speed can path through the private region. Thus, carbons dissociated from CD_4 emitted at the outer strike point are also spread out along the separatrix. When the sticking coefficient at the dome is very small, the dome enhances the contamination of hydrocarbon into the main plasma. The dissociation process cannot be simplified down to ionization process of carbon with low energy, in the attached divertor plasma.

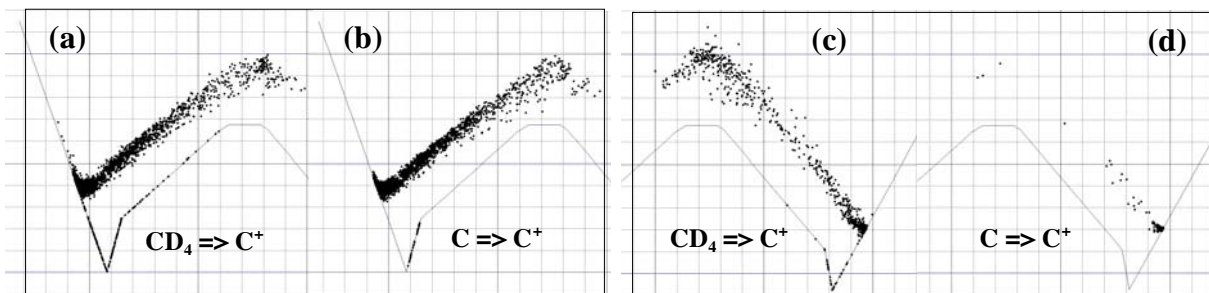


FIG. 3 Birth positions of C^+ ions (a,c) dissociated from methane, and (b,d) ionized from carbon. They are sputtered (a,b) from the inner strike point (detached state) and (c,d) from the outer strike point (attached state). The sticking coefficient is assumed to be 0.

5. Kinetic Effect of Thermal Force on Impurity Retention

The impurity retention in the divertor region is basically determined by the balance between the thermal force (toward hotter region in fluid approximation) and the friction force (toward divertor plates). The kinetic thermal force has opposite direction of fluid type according to impurity speed, as shown in Fig. 1. When the speed of an impurity is much smaller than the ion thermal speed, $V_I \ll v_{thi}$, the number of plasma ions strongly interacting with the impurity

ion decreases with the ion temperature ($\delta f/\delta T_i < 0$; f : ion distribution function). On the contrary, when $V_I \sim v_{thi}$, the number of those ions increases with T_i ($\delta f/\delta T_i > 0$). This is why the direction of the kinetic thermal force turns over. This kinetic effect appears for impurity with a high speed, i.e. light impurity. For detached divertor plasma of JT-60SA [13], simulations of He transport were carried out [10]. In the present paper, the effect of kinetic thermal force on He transport is further investigated. The background plasma parameters are calculated with the SOLDOR/NEUT2D code for the divertor configuration with “V-shaped corner” shown in Fig. 5(a). The heat flux and the particle flux from the core edge ($r/a=0.95$) are specified, $Q_{total}=37$ MW, $\Gamma_i=5 \times 10^{21} \text{ s}^{-1}$. We employ $D_{\perp}=0.25 \text{ m}^2/\text{s}$ and $\chi_{\perp}^i=\chi_{\perp}^e=1 \text{ m}^2/\text{s}$ for the cross-field diffusion coefficients. The pumping speed of $S_{pump}=50 \text{ m}^3/\text{s}$ is specified at the cryopanel. The gas puff of $\Gamma_{puff}=5 \times 10^{21} \text{ s}^{-1}$ is required to obtain plasma detachment near the outer strike point.

The He^{2+} ions are assumed to inflow across the core edge uniformly. The He^{2+} flux is assumed to be small and not to influence the background plasma. Each test particle of He^{2+} ion has a velocity chosen from the Maxwellian distribution with the plasma ion temperature at the core edge. In the present simulations, ionization and recombination processes are included, but the elastic scattering and charge exchange processes are not included for simplicity. Firstly, we investigate the effect of the kinetic thermal force on the He compression, under the condition of excluding the recycling at the divertor plate and the walls. Figure 4 shows the He density profile in a flux tube close to the separatrix surface. The kinetic effect of the thermal force is found to increase the He density in the divertor region by a factor of ~ 2 , compared with the conventional (fluid) evaluation. The recombination process becomes dominant at the front of the divertor plate due to high density and low electron temperature ($n_{ed} > 2 \times 10^{21} \text{ m}^{-3}$, $T_{ed} \sim 1 \text{ eV}$) and the He^{2+} density decreases abruptly there. Figures 5(b) and (c) show the distributions of number density of test particles hitting on the divertor along the inner vertical target and the outer vertical target, respectively. The test particles which move along the separatrix are pushed upstream by the friction force of reverse plasma flow and the thermal force. A few test particles can move into the divertor region and they are pushed downstream by the kinetic thermal force because the speed is much higher than the ion thermal speed. As a result, the number of particles to reach the targets increases near the strike point, compared to the case applied the fluid thermal force. The region where large difference appears ($Z < -2.30 \text{ m}$ in Fig. 5(b), $Z < -2.46 \text{ m}$ in Fig. 5(c)) corresponds to that where the flow becomes reverse near upstream the X-point.

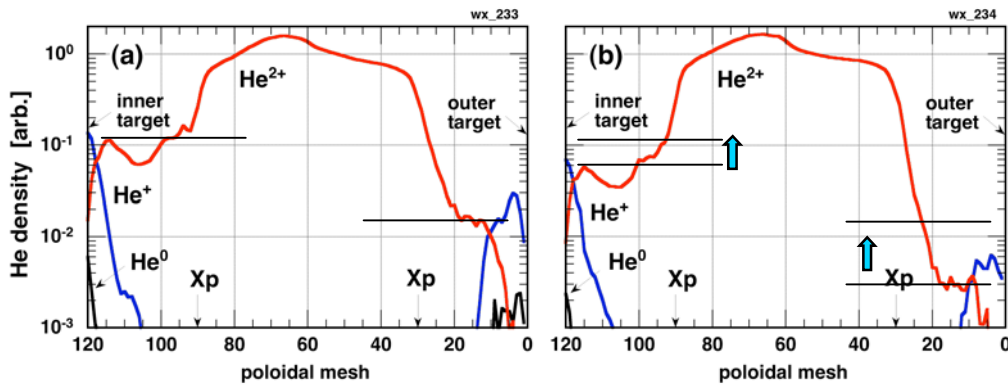


Fig. 4 He^{2+} density profile in the flux tube close to the separatrix surface. Under the condition of excluding recycling process at the targets and walls, IMPMC calculations are carried out using (a) the kinetic thermal force and (b) the fluid thermal force. Note that the kinetic thermal force pushes some He ions with high speeds into the divertor region.

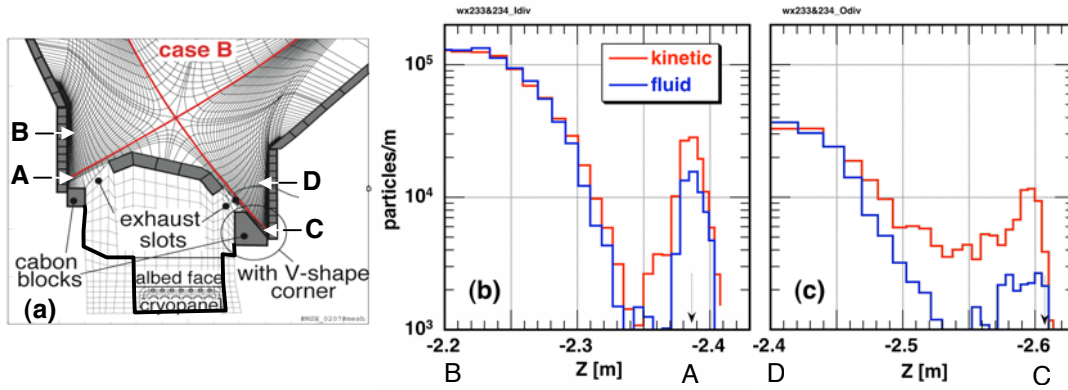


FIG. 5 (a) Divertor configuration of JT-60SA with “V-shaped Corner” and mesh used in the simulations. (b) Number density of test particles to hit on the inner vertical target. (c) Number density of test particles to hit on the outer vertical target. Red lines and blue lines indicate the results using the kinetic and fluid thermal force, respectively.

Secondly, a model of recycling at the divertor plate is incorporated into simulations and the total effect of the kinetic thermal force on the He transport is investigated. In the recycling model, a He neutral is emitted with an energy determined from the particle and energy reflection coefficients [14]. The thermalization process of He ion ionized after recycling is simulated by Monte-Carlo method, in contrast to the fluid modelling with the assumption of instantaneous thermalization of impurity ions. The kinetic effect is masked by the recycling at the target plates, as shown in Fig. 6. The energies of He ions which originate from the targets are small and are nearly equal to those of plasma ions due to short slowing down time, i.e. 1 ~ several eV in the divertor region. Thus, the effect of the kinetic thermal force becomes negligible. Total amount of test particles in the inner and outer divertor region increases by 15% and 21 %, respectively. This change might enhance the recycling further, depending on the flow patterns near the X-point and the temperature profile along the magnetic field line. In such case, the kinetic thermal force could have a perceptible effect on the He density. The elastic scattering of He neutral with proton collision affects the He transport [15]. The code improvement to incorporate the elastic scattering model and simulation studies for various flow patterns are required for the reliable evaluation of the He ash exhaust.

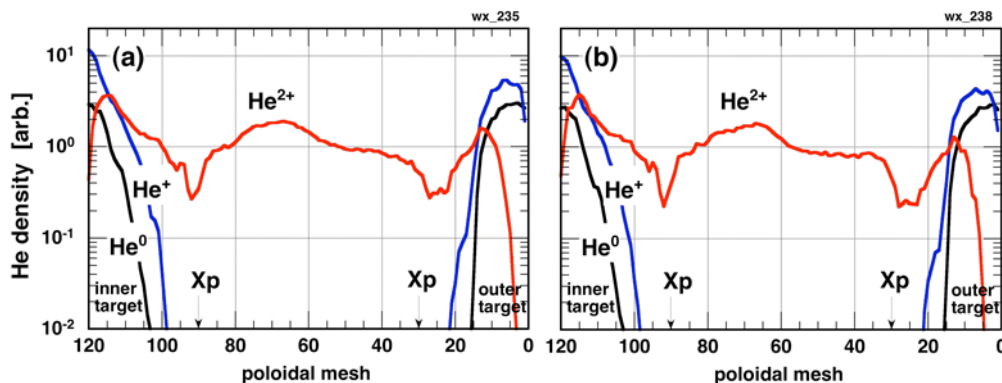


FIG. 6 He^{2+} density profile in the flux tube close to the separatrix surface. Under the condition of including recycling process at the targets and walls, IMPMC calculations are carried out using (a) the kinetic thermal force and (b) the fluid thermal force.

6. Summary

The Monte-Carlo modelling (MC) for impurity transport is required in order to take into account the kinetic effect or the complex dissociation processes of hydrocarbon. The self-

consistent coupling of an impurity MC code with a divertor code is a hard task due to long computational time and MC noise. We have solved these intrinsic problems of MC modelling by developing the new diffusion model for scattering process, optimizing on the massive parallel computer and developing a particle reduction scheme. Thereby the self-consistent coupling of the impurity MC code IMPMC to the divertor code SOLDOR/ NEUT2D have been developed. Using this integrated code with a simplified dissociation model of hydrocarbons, the dynamic evolution of an X-point MARFE observed in JT-60U is investigated. The code reproduce well the characteristics of the X-point MARFE and clarify that the radiation near the X-point during MARFE originates in neutral carbons chemically sputtered from the private region. The EDDY/IMPMC code of a full dissociation modelling for hydrocarbons confirms that the dome with zero sticking coefficient enhances the contamination of hydrocarbon into the main plasma and that the dissociation process cannot be simplified down to ionization process of carbon with low energy, especially in the attached divertor plasma. The kinetic effect of thermal force on the He transport is investigated for the V-shaped corner divertor configuration of JT-60SA. The kinetic thermal force has an effect on the He ions: some of them are pushed from the SOL into the divertor region against the reverse plasma flow near the X-point. As a result, the He compression is improved. However, this effect is masked by the recycling at the target. Further simulation studies are required for various flow patterns.

Acknowledgement

They are indebted to Drs. T. Ozeki and M. Kikuchi for their continuous encouragement. This work is partly supported by the Grant-in-Aid for Scientific Research on Priority Areas of MEXT (19055005) and by the Grant-in-Aid for Scientific Research (B) of JSPS (18360448).

References

- [1] Progress in the ITER Physics Basis: Chapter 4, Nucl. Fusion **47** (2007) s203.
- [2] SHIMIZU, K., TAKIZUKA, T., et al, J. Nucl. Mater. **241-243** (1997) 167.
- [3] SHIMIZU, K., TAKIZUKA, T., et al, J. Nucl. Mater. **363-365** (2007) 426.
- [4] SHIMIZU, K., TAKIZUKA, T., et al, Contrib. Plasma Phys. **48** (2008) 270.
- [5] SHIMIZU, K., KUBO, H., et al., J. Nucl. Mater. **220-222** (1995) 410.
- [6] SHIMIZU, K., TAKIZUKA, T., et al., J. Nucl. Mater. **313-316** (2003) 1277.
- [7] OHYA, K., INAI, K., et al, J. Nucl. Mater. **363-365** (2007) 78.
- [8] JANEV, R.K., REITER, D., "Collision processes of hydrocarbon species in hydrogen plasmas: I. The methane family", Report Forschungszentrum Julich, Jul-3966 (2002).
- [9] REISER, D., REITER, D., et al, Nucl. Fusion **38** (1998) 165.
- [10] SHIMIZU, K., Takizuka, T., et al., PSI-18 (2008), submitted to J. Nucl. Mater.
- [11] Braginskii, S.I., et al., Soviet Phys. JETP **6** (1958) 358.
- [12] KONOSHIMA, S., TAMAI, H., et al., J. Nucl. Mater. **313-316** (2003) 888.
- [13] KAWASHIMA, H., et al., ISFNT-8 (2007), to be published in Fus. Eng. Des. (2008).
- [14] RUZIC, D.N., JULIANO, D.R., J. Nucl. Mater. **196-198** (1992) 194.
- [15] KUBO, H., TAKENAGA, H., et al., Plasma Phys. Control. Fusion **41** (1999) 747.